



Published in final edited form as:

Bioorg Med Chem. 2017 October 15; 25(20): 5194–5202. doi:10.1016/j.bmc.2017.07.020.

## Picomolar inhibition of $\beta$ -galactosidase (bovine liver) attributed to loop closure

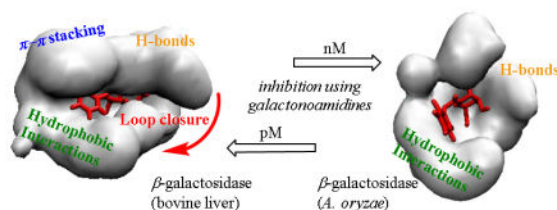
Jessica B. Pickens, Feng Wang, and Susanne Striegler

University of Arkansas, Department of Chemistry and Biochemistry, 345 N Campus Drive, Fayetteville, AR 72701, USA

### Abstract

In an effort to examine similarities in the active sites of glycosidases within the GH35 family, we performed a structure-activity-relationship study using our recently described library of galactonoamidines. The kinetic evaluation based on UV/Vis spectroscopy disclosed inhibition of  $\beta$ -galactosidase (bovine liver) in the picomolar concentration range indicating significantly higher inhibitor affinity than previously determined for  $\beta$ -galactosidase (*A. oryzae*). Possible alterations in the secondary protein structure or folding were excluded after further examination of the inhibitor binding using CD spectroscopy. Molecular dynamics studies suggested loop closing interactions as a rationale for the disparity of the active sites in the  $\beta$ -galactosidases under investigation.

### Graphical Abstract



### Keywords

inhibition;  $\beta$ -galactosidase; Amidine; carbohydrate

This manuscript version is made available under the CC BY-NC-ND 4.0 license.

#### Supplementary Material

Experimental details for all molecular dynamic simulations of the interactions of **1a**, **1v** and **1x** with the  $\beta$ -galactosidases under investigation; the constructed pdb file for the anticipated structure of  $\beta$ -galactosidase (bovine liver); and the QMEAN6 scores for all models returned from the Robetta server are available at <http://dx.doi.org/10.1016/j.bmc>.

**Publisher's Disclaimer:** This is a PDF file of an unedited manuscript that has been accepted for publication. As a service to our customers we are providing this early version of the manuscript. The manuscript will undergo copyediting, typesetting, and review of the resulting proof before it is published in its final citable form. Please note that during the production process errors may be discovered which could affect the content, and all legal disclaimers that apply to the journal pertain.

## 1. Introduction

Approximately 1% of all genes known to date code for glycoside hydrolases [3.2.1] documenting their ubiquity in Nature.[1] Glycoside hydrolases are divided into 14 clans based on structural similarities, and then further subdivided into 130 families based on reaction mechanisms, evolutionary relationships, and substrate specificity.[2] All  $\beta$ -galactosidases [3.2.1.23] belong to clan A and contain an ( $\alpha/\beta$ )<sup>8</sup> (TIM) barrel as catalytic domain. Two glutamic acid residues are located in  $\beta$ -strands four and seven of this TIM barrel and act as acid-base donor and nucleophile during catalytic turnover.[3]

$\beta$ -Galactosidases are isolated from plants,[4] fungi,[5] bacteria,[6], and mammalian tissue, [7] and are found in four families of glycoside hydrolases (GH), namely GH-1, GH-2, GH-35, and GH-42.[8] Currently, about 1700 glycoside hydrolases are assigned to GH-35 including  $\beta$ -galactosidases,[9] exo- $\beta$ -glucosaminidases, exo- $\beta$ -1,4-galactanases and  $\beta$ -1,3-galactosidases. Among those, about 700  $\beta$ -galactosidases are known,[9] but only 10 of them are structurally characterized using X-ray diffraction.[10] In the absence of structural data, information on stabilizing forces in the active site of an enzyme has been deduced from spectroscopic data.[11] The characterization of stabilizing forces between inhibitors and  $\beta$ -galactosidases may lead to the discovery of new therapeutics for diseases associated with these enzymes, such as lysosomal disorders,[12] diabetes,[13] and several neurological disorders.[14]

In this context, we set out to elaborate the differences and similarities during catalytic glycoside hydrolysis of  $\beta$ -galactosidases from *A. oryzae* (4IUG)[5] and bovine liver, using UV/vis and CD spectroscopy. Both enzymes belong to GH-35 and cleave exo- $\beta$ -D-galactopyranosyl residues from oligosaccharides or other glycoconjugates in a retaining fashion.[15] Our spectroscopic results disclose distinct differences between the two  $\beta$ -galactosidases. Molecular dynamic studies suggest contributions of a loop closure for the  $\beta$ -galactosidase from bovine liver as stabilizing interaction within its active site.

## 2. Results and discussion

Our previous structure-activity relationship (SAR) studies using a library of galactonoamidines **1a–y** (Chart 1) characterized all synthesized compounds as competitive inhibitors and revealed nanomolar inhibition of the catalytic activity toward  $\beta$ -galactosidase (*A. oryzae*).[16–18] The combined results indicated hydrophobic interactions with the aglycon,[16–18] and H-bonds with the glycon as a driving force for the interactions between inhibitors and amino acids within the active site. Similar results were expected for the inhibition of  $\beta$ -galactosidase from bovine liver that is classified in the same glycoside hydrolase family based on sequence similarity and mechanism. However, the extended SAR studies revealed distinct differences between the two  $\beta$ -galactosidases indicating altered support of inhibitor binding that caught our attention for an in-depth investigation. In absence of structural data, we hypothesized that a combination of  $\pi$ - $\pi$  stacking, hydrophobic and possibly loop closure interactions, cause the noted dramatic difference in the inhibition of galactonoamidines toward the selected  $\beta$ -galactosidases. The details of the study are summarized and discussed below.

## 2.1. Structure-activity relationship

While glyconoamidines exist in tautomeric forms with endo- or exocyclic double bonds in a solution of organic solvents depending on their structure, the compounds are protonated under assay conditions in aqueous solution.[19] The resulting positive charge is delocalized (Chart 1).

Notably, a small number of galactonoamidines with aromatic and aliphatic aglycons (**1d**, **1m**, **1p–r**) showed comparable efficacy toward both enzymes rendering them efficient inhibitors of either hydrolase (Figure 1a). The efficacy of all other inhibitors **1** is remarkably higher toward  $\beta$ -galactosidase (bovine liver) than for  $\beta$ -galactosidase (*A. oryzae*) (Table 1, Figure 1b).[16]

The results suggest different stabilization of the corresponding inhibitor binding in the active sites of the two monomeric  $\beta$ -galactosidases under investigation but do not disclose the source of this discrimination. All studied galactonoamidines **1a–y** were characterized as competitive inhibitors toward both  $\beta$ -galactosidases using Lineweaver-Burk, Dixon and Eddie-Hofstee plots, and representative examples using **1a** are depicted (Figures 2a & b). All kinetic data were analyzed by non-linear regression applying the Michaelis-Menten model. Apparent catalytic rate constants ( $k_{cat}$  and  $k'_{cat}$ ) and affinity constants ( $K_M$  and  $K'_M$ ) were determined in absence and presence of galactonoamidines **1a–y**. The inhibition constants ( $K_i$ ) (Tables 1 & 2) were deduced from these data by standard methods.[20]

Analysis of the inhibition constants reveals that the affinity of any inhibitor **1** is about two orders of magnitude higher toward  $\beta$ -galactosidase (bovine liver) than toward  $\beta$ -galactosidase (*A. oryzae*). The resulting inhibition constants are in the picomolar instead of nanomolar concentration range. Consequently, the active site of the  $\beta$ -galactosidase (bovine liver) must support the inhibitor binding substantially better than that of  $\beta$ -galactosidase (*A. oryzae*). A synergy of H-bond interactions,  $\pi$ - $\pi$  stacking, and hydrophobic interactions alone is unlikely to serve as a rationale to sufficiently explain this observation. Additional interactions, such as distorted protein folding upon inhibitor binding, or loop closure-supported catalysis may be present, which has been previously noted for other proteins with TIM barrels.[21–24] Further experiments using CD spectroscopy were therefore conducted to illuminate the inhibitor binding in the active sites of the  $\beta$ -galactosidases.

## 2.2. Effect of inhibitor binding on protein folding evaluated by circular dichroism spectroscopy

A possible influence of the inhibitor binding on protein structure and folding of both glycosidases was explored using CD spectroscopy with selected inhibitors. Amidine **1a** was employed as the lead compound as it showed overall the lowest inhibition constant ( $K_i = 50 \pm 10$  pM) reflecting the highest binding affinity upon interacting with  $\beta$ -galactosidase (bovine liver). Amidine **1v** was selected as an example for an inhibitor with modified glycon, and amidine **1x** was chosen as a control compound without aglycon (for structures of **1v** and **1x**, see Table 2). The CD spectra of all assemblies between  $\beta$ -galactosidase (bovine liver) and inhibitors reveal only minor changes in the observed molar ellipticity ( $\lambda_{max} = 225 \pm 3$  nm) (Figure 3).

This observation indicates an unaltered three-dimensional structure of the enzyme and unaffected folding pattern upon coordination of the selected galactonoamidines. Similar conclusions were drawn by others for related studies.[25, 26] Consequently, alterations in the protein folding are unlikely to cause the observed strong inhibitor binding. The CD spectra obtained from interactions between the selected inhibitors and  $\beta$ -galactosidase (*A. oryzae*) are likewise unaffected.

Unfortunately, our attempts to derive and predict three-dimensional structures from the measured CD data by taking advantage of previously developed programs, K2D3[27] and BESTsel,[28] were futile. This conclusion was reached after comparing the identified amounts of  $\alpha$ -helices and  $\beta$ -sheets of the published structure for  $\beta$ -galactosidase (*A. oryzae*) [5] to computed data derived from the measured CD data. The high amount of  $\beta$ -sheets determined by X-ray diffraction is not calculated correctly. Similar problems were noted by other researchers on similar occasion previously.[28] Consequently, the corresponding CD data were not analyzed further. Instead, molecular dynamic studies were performed in an attempt to provide a rationale for the drastically different affinity of the galactonoamidines upon binding to the selected enzymes.

### 2.3. Effect of inhibitor binding on protein folding evaluated by molecular dynamics studies

While the structure of  $\beta$ -galactosidase (*A. oryzae*) (4IUG)[5] is available in the Protein Database, the three-dimensional structure of  $\beta$ -galactosidase (bovine liver) is still unknown. Therefore, we constructed a model of this enzyme based on homology-based comparative modeling using the Robetta server.[29] Predicting a protein structure from an amino acid sequence is a grand challenge. While the Rosetta suite of programs used by the Robetta server is considered the state-of-the-art,[30] we are well aware of the limitations of our approach. In this specific case, however, we do benefit from the high degree of homology between  $\beta$ -galactosidase (bovine liver, Q58D55) and  $\beta$ -galactosidase (*Homo sapiens*, P16278), for which the solid state structure has been determined by X-ray diffraction (3wf3). In addition, we noted almost identical structures around the active site for the five highest-ranked models returned by the Robetta server. For example, the maximum root mean square error (RMSE) is 0.13 Å for all residues within a 20 Å distance from the active site for the five homology models. Such a good structural agreement is probably due to a very good sequence homology with  $\beta$ -galactosidase (*H. sapiens*) near the active site, as to be expected for enzymes classified in the same GH family.[3]

To examine the quality of the predictions, each model was submitted to the Quality Modeling Energy Analysis (QMEAN) server.[31] An estimate of the model reliability was produced as QMEAN6 score by a combination of 6 linear terms into a composite score (0–1).[32] The structure selected for further analysis had a composite QMEAN6 score of 0.98 indicating a model with a high level of confidence. A BLAST comparison between our model for  $\beta$ -galactosidase (bovine liver) and  $\beta$ -galactosidase (*H. sapiens*) reveals 518 identical and 73 very similar amino acid residues indicating in a sequence similarity of 90.5 %.

Initially, we performed docking predictions using AutoDock Vina with the inhibitors **1a**, **1v** and **1x** in the active sites of the  $\beta$ -galactosidases from bovine liver and *A. oryzae*. However,

the predicted free energies of the docked conformations did not differ significantly and thus did not disclose a rationale for the experimentally observed superior binding of the inhibitors in the active site of  $\beta$ -galactosidase (bovine liver). Therefore, molecular dynamic studies based on GROMACS were used instead to characterize the inhibitor binding.[33] Interactions with catalytic amino acid residues,  $\pi$ - $\pi$  stacking promoting aromatic amino acids, and the relative number of H-bond interactions are highlighted. Similar studies to clarify interactions between enzymes and carbohydrate analogs were reported by others recently.[34, 35]

The modeling study suggests that amidine **1a** interacts with both catalytic residues of  $\beta$ -galactosidase (bovine liver), namely the proton donor Glu-187 and the nucleophile Glu-267. The modeling suggests that amidine **1v** does not stay in the active site, and interacts with Glu-267 only due to steric hindrance. Amidine **1x** interacts with both catalytic residues as well, but to some lesser extent as discussed below. Other researchers have previously speculated that two binding pockets exist within the active site of  $\beta$ -galactosidase (bovine liver) to support interactions with the glycon and the aglycon of inhibitors and substrates. [36] Our molecular dynamic studies support this hypothesis and disclose initial binding of the *glycon* of **1a** in one of the binding pockets in the active site followed by binding of its *aglycon* with subsequent loop closure (Figure 4).

This loop closure occurs via a CH- $\pi$  stacking interaction between Trp272 and Tyr484 after the induced fit of **1a** in the active site (for a movie, see Supporting Information). Its binding is further supported by  $\pi$ - $\pi$  stacking interactions of its aglycon with Trp272 and Tyr484 (Figure 4). Additionally, inhibitor **1a** shows the highest number of H-bond interactions toward amino acids of both  $\beta$ -galactosidases under investigation (Figures 5a & 7a). The corresponding images display well-embedded inhibitor structures (Figures 6a & 8a). However, the modeling study implies that the aglycon of **1a** is nested within a closed loop of  $\beta$ -galactosidase (bovine liver) (Figure 6a), while the active site in  $\beta$ -galactosidase (*A. oryzae*) remains open (Figure 8a). Similar loop closing interactions were previously reported by others, e.g. for  $\beta$ -galactosidase (*E. coli*), [6, 37, 38] but were not noted for  $\beta$ -galactosidase (bovine liver) yet.

Although the initial docking study suggests **1v** to bind within the active site during the initial docking studies in a similar fashion as the other selected inhibitors, **1v** moves out of the active site during the energy minimization with the GROMOS model. As a result, inhibitor **1v** stabilizes in a flipped and twisted orientation relative to the other inhibitors only *partially within* the active site showing  $\pi$ - $\pi$  stacking interactions with Tyr269 (Figure 6b). This shift causes the inhibitor to interact with only one of the two catalytic residues, namely Glu-267, throughout the entire 30ns simulation. The experimentally determined inhibition constants (see above) indicate a 30,000-fold higher affinity for **1a** over **1v**. The result is echoed by the observations of the modeling study. Similar conclusions on inhibitor binding in presence of steric hindrance were also previously reported by us and others.[39–41] Additionally, the frequency of H-bond interactions between  $\beta$ -galactosidase (bovine liver) and galactonoamidine **1v** is only slightly smaller than for **1a** (Figure 5b). As **1x** is a control compound lacking the aglycon of **1a** and **1v**, the corresponding aglycon binding site remains unoccupied (Figure 5C), and the loop closure is incomplete. The modeling study

furthermore reveals that the number of H-bond interactions is overall reduced once a control compound without aglycon is employed (**1x**, Figures 5c & 7c).

The inhibitor binding toward  $\beta$ -galactosidase (*A. oryzae*) appears to be driven slightly differently. In short, interactions of amidines **1a** and **1x** with both catalytic residues are noted; Glu-200 (proton donor) and Glu-298 (nucleophile). Steric hindrance implemented at C-2 of the glycon allows amidine **1v** to interact only with the nucleophilic amino acid Glu-298. In contrast to above-described interactions within  $\beta$ -galactosidase (bovine liver), inhibitor **1v** binds *within* the active site of  $\beta$ -galactosidase (*A. oryzae*) and assumes a different orientation than **1a** (Figure 8b). At the same time, the number and frequency of H-bond interactions are significantly lower for amidine **1v** than for its parent **1a** (Figure 6b).

The combined modeling results provide a rationale for the experimentally observed picomolar inhibition of  $\beta$ -galactosidase (bovine liver) by galactonoamidines **1** compared to weaker nanomolar inhibition toward  $\beta$ -galactosidase (*A. oryzae*). While the amidines use H-bond interactions for stabilization of the glycon in both glycosidases, a combination of a closed loop,  $\pi$ - $\pi$ -stacking, and hydrophobic interactions is apparent for galactonoamidine binding toward  $\beta$ -galactosidase (bovine liver).

### 3. Conclusions

Two  $\beta$ -galactosidases from the same glycoside hydrolase family (GH35) were evaluated upon their interactions with galactonoamidines to compare the efficiency of their active sites. Given the enzyme classification based on structure and mechanism similarities, comparable interactions and inhibition ability were initially expected. All compounds were found to be competitive inhibitors towards both glycosidases. However, SAR studies using UV/vis spectroscopy revealed inhibition in the picomolar concentration range toward  $\beta$ -galactosidase (bovine liver) that is two order of magnitude stronger than previously determined inhibition of the same inhibitors toward  $\beta$ -galactosidase (*A. oryzae*). Galactonoamidine **1a** was identified as the most potent inhibitor toward both  $\beta$ -galactosidases. CD spectroscopy revealed insignificant alterations of the protein structure upon inhibitor binding that does not account for the noted significant difference in inhibitor potency. Molecular modeling studies using **1a**, **1v** and **1x** suggested loop closure and  $\pi$ - $\pi$  stacking interactions in addition to hydrophobic interactions and H-bond formation as a rationale for the considerably higher affinity of the galactonoamidine inhibitors toward  $\beta$ -galactosidase (bovine liver). By contrast, only hydrophobic interactions and H-bond formation support the binding of galactonoamidines to  $\beta$ -galactosidase (*A. oryzae*).

## 4. Experimental

### 4.1. Instrumentation

UV/Vis data were recorded on a FilterMax F5 Multi-Mode Microplate Reader from Molecular Devices using 96-well, medium-binding microton ELISA-plates from Greiner Bio-one. CD spectra were recorded on a Jasco J-1500 CD Spectrometer Model 150 with EXOS liquid cooling system from Koolance Inc. with the supplied Spectra Manager software Version 2.12.00 using a Fisher Scientific Suprasil quartz microcell with 500  $\mu$ L

capacity, 45 mm height, and an optical path length  $l$  of 10 mm. All pH values were obtained using a Beckman  $\Phi$  250 pH meter equipped with a refillable ROSS combination pH electrode from Orion with epoxy body and an 8 mm semi-micro tip. Nanopure water at a resistance of 18.2 m $\Omega$  was obtained from a ThermoScientific Barnstead E-pure™ water purification system.

## 4.2. Materials and Methods

**4.2.1. Chemicals**— $\beta$ -galactosidases from bovine liver and *Aspergillus oryzae* were obtained from Sigma-Aldrich and stored at  $-18$  °C until use. Metal-free sodium hydroxide at 99.999 % purity and HEPES buffer were purchased from Sigma-Aldrich and used as received. All buffer solutions were prepared by standard methods at ambient temperature accounting for temperature differences at their intended use. All galactonoamidines were synthesized as described previously.[16]

### 4.2.2. UV/Vis spectroscopy

#### 4.2.2.1. Assays using $\beta$ -galactosidase (bovine liver)

**4.2.2.1.1. Enzyme stock solution:** The commercially obtained lyophilized powder of  $\beta$ -galactosidase (bovine liver) was dissolved in 5 mL HEPES buffer and stored in 50  $\mu$ L aliquots at  $-80$  °C until use. A BCA assay revealed a protein content of  $93.5591 \pm 4.18745$   $\mu$ g/mL that translates into a  $139.64 \pm 6.25$   $\mu$ M protein concentration of the solution ( $M = 67,000$  g mol $^{-1}$ ).[7, 42]

For determination of IC<sub>50</sub> values, a 50  $\mu$ L aliquot of the frozen enzyme solution was thawed, diluted into 5 mL with 5 mM HEPES buffer and stored on ice until use. For determination of inhibition constants, a 20  $\mu$ L aliquot of the frozen protein solution was used and diluted in identical fashion.

**4.2.2.1.2. Substrate stock solution:** Substrate stock solutions for the determination of IC<sub>50</sub> values were prepared by dissolving 9.15–9.62 mg (0.030–0.032 mmol) of 4-nitrophenyl- $\beta$ -D-galactopyranoside in 5 mL of 5 mM HEPES buffer immediately prior to use. Stock solutions for the determination of inhibition constants were prepared likewise using 9.98–10.27 mg (0.033–0.034 mmol) of the same substrate in 10 mL of buffer solution.

**4.2.2.1.3. Inhibitor stock solution:** Appropriate aliquots of a 500  $\mu$ M aqueous solution of the galactonoamidines **1a–y** were diluted with nanopure water yielding 0.005, 0.05, 0.125, 0.25, 0.5, 2.5, 10, 20, 30, 50, 100, and 200  $\mu$ M inhibitor stock solutions that were stored at ambient temperature until use. For the determination of IC<sub>50</sub> values, 11 of those solutions with different inhibitor concentrations were used in 10  $\mu$ L aliquots. For the determination of K<sub>i</sub> values, 2 or more solutions with concentrations between 0.5 and 1.5 nM (**1a**, **1c–d**, **1f–j**, **1l–m**, **1o–r**), 1 and 2 nM (**1b**, **1k**, **1n**, **1s–t**), 5 and 6 nM (**1u**), 2,500 and 10,000 nM (**1v–w**), 10,000 and 20,000 nM (**1x**), 5,000–50,000 nM (**1y**) were used,

**4.2.2.1.4. As say t o determine IC<sub>50</sub> values:** Typically, a 10  $\mu$ L aliquot for each of 11 different inhibitor stock solutions was mixed with 30  $\mu$ L substrate stock solution and 20  $\mu$ L of the buffer solution in a 96-well plate. After equilibration at 30 °C over 30 min, a 40  $\mu$ L

aliquot of the enzyme stock solution was added. The resulting solutions were thoroughly mixed, and the change in absorbance followed at 405 nm over 240 min in 10 min intervals. In a control experiment, the aliquot of the inhibitor solution was replaced by the same amount of buffer solution. All experiments were done as duplicates.

**4.2.2.1.5. Data analysis to determine  $IC_{50}$  values:** The final absorbance read for the enzymatic substrate hydrolysis in presence and absence of inhibitor were transferred into percentages of overall inhibition, and plotted against the inhibitor concentration in logarithmic scale.

**4.2.2.1.6. Assay to determine  $K_i$  values:** Typically, a 0–70  $\mu\text{L}$  aliquot of the substrate stock solution was pipetted in 96-well plates in 10  $\mu\text{L}$  increments, a constant 10  $\mu\text{L}$  aliquot of the inhibitor stock solution was added, and the nominal volume of all solutions increased to 80  $\mu\text{L}$  with appropriate amounts of buffer solution. The resulting solutions were equilibrated at 30 °C for 30 min prior to addition of a constant 20  $\mu\text{L}$  aliquot of enzyme stock solution. All solutions were thoroughly mixed, and the change of absorbance was read immediately at 405 nm for 45 min in 27s intervals. All experiments were performed in duplicate or more.

**4.2.2.1.7. Data analysis to determine  $K_i$  values:** The measured change in absorbance was plotted over time in presence and absence of inhibitor to determine the initial rate of the substrate hydrolysis and transformed into concentration by using the apparent extinction coefficient for 4-nitrophenolate at pH 7.5 in 5 mM HEPES buffer and a total volume of 100  $\mu\text{L}$  ( $\epsilon_{\text{mol}} = 13,300 \pm 60 \text{ M}^{-1} \text{ cm}^{-1}$ ). The obtained initial rates were corrected for enzyme concentration and graphed as a function of the respective substrate concentration. The resulting hyperbolic data were fitted by non-linear regression to determine apparent Michaelis-Menten constants ( $K_m$  and  $K'_m$ ) and rate constants ( $k_{\text{cat}}$  and  $k'_{\text{cat}}$ ) in absence and presence of inhibitors, respectively. All experiments were conducted in duplicate, and the data were averaged. Kinetic parameters for at least two different inhibitor concentrations were determined, and Lineweaver-Burk plots ( $[E]/\text{rate}$  vs  $1/[S]$ ) constructed to visualize and examine the inhibition type. The inhibition constant ( $K_i$ ) for competitive inhibition was then calculated from equation (1):

$$K'_m = K_m \times (1 + ([I]/K_i)) \quad (1)$$

**4.2.2.2. Assays using  $\beta$ -galactosidase (*A. oryzae*):** The experimental procedure describing the cleavage of 2-chloro-4-nitrophenyl  $\beta$ -D-galactopyranoside by  $\beta$ -galactosidase (*A. oryzae*) and the inhibition of this reaction in the presence of galactonoamidines **1a–y** is described in detail elsewhere.[16, 17, 43] The developed assays were used for selected inhibitors to determine kinetic parameters, inhibition constants, and  $IC_{50}$  values as described.



### 4.2.3. CD spectroscopy

**4.2.3.1. Enzyme stock solution:** Typically, an aliquot of the above-described  $\beta$ -galactosidase (bovine liver) solution was thawed and diluted to 5 mL with 5 mM HEPES buffer yielding an enzyme stock solution that was kept on ice until use.

**4.2.3.2. Inhibitor stock solutions:** Solutions of **1a**, **1v**, and **1y** were prepared by dissolving 3–5 mg of the freeze-dried compound in 10 mL of nanopure water in volumetric flasks. Subsequent serial dilutions of 30–50  $\mu$ L aliquots afforded 100  $\mu$ M stock solutions of the respective inhibitors that were stored at ambient temperature prior to use.

**4.2.3.3. Assay to measure ellipticity:** Typically, 250  $\mu$ L of the enzyme stock solution was mixed with the same volume of 100 mM inhibitor stock solution. After equilibration, the ellipticity of the resulting solution was measured between 190–275 nm with a resolution of 0.5 nm, and the data from 5 accumulation scans were averaged. The resulting data were adjusted for contributions of unbound inhibitor and buffer effects by background corrections prior to data analysis.

**4.2.3.4. Data analysis:** The measured specific rotation of the circularly polarized light  $\theta$  [mdeg] was transformed into molar ellipticity  $[\theta]$  in  $[\text{deg M}^{-1} \text{m}^{-1}]$  by using equation (1),

$$[\theta] = \theta \times 100 / (c \times l) \quad (1)$$

the molar extinction coefficient  $\epsilon$  in  $[\text{deg M}^{-1} \text{m}^{-1}]$  by using equation (2),

$$\Delta\epsilon = [\theta] / 3298.2 \quad (2)$$

and the mean residue molar ellipticity  $[\theta]_{\text{MR}}$   $[\text{deg M}^{-1} \text{m}^{-1} \text{residue}^{-1}]$  by using equation (3),

$$[\theta]_{\text{MR}} = [\theta] / N; \quad (3)$$

$\theta$  represents the ellipticity in degree,  $c$  the molar protein concentration,  $l$  the optical pathlength [cm] and  $N$  the number of residues in the protein ( $N=653$ [44] and  $1005$ [45], respectively). The resulting rotation data were smoothed by a 7-point Savitzky-Golay filter and plotted against the wavelength  $\lambda$  [nm].

**4.2.4. Molecular Dynamics**—The structure of  $\beta$ -galactosidase (bovine liver) is not known yet, and was thus predicted through comparative modeling using the Robetta server and the known structure of  $\beta$ -galactosidase (*H. sapiens*).[29] Out of the five highest-ranked models returned, one was selected for further analysis based on its QMEAN6 score of 0.98, which indicates a very high quality prediction.[31] The structure of  $\beta$ -galactosidase (*A. oryzae*, 4IUG) was obtained from the Protein Data Bank (<http://www.rcsb.org/pdb/>).[10] All

water molecules, solvents, and substrates were removed from the structure file prior to processing simulations.

#### **4.2.4.1. Docking studies of glycosidases with coordinated galactonoamidine**

**inhibitors:** Mol files of the galactonoamidine inhibitors were initially converted into pdb files using PYMOL,[46] and then transferred into pdbqt files that allow all non-ring bonds to rotate during docking with the Python Molecular Viewer, vers. 1.5.6.[47] Likewise, the coordinates of the enzymes were transferred from pdb into pdbqt files after addition of Kollman charges using AutoDock Tools.[48] A  $30 \times 30 \times 30 \text{ \AA}^3$  grid box was set at the center of the active site of  $\alpha$ -galactosidase (*A. oryzae*), while a  $15 \times 15 \times 15 \text{ \AA}^3$  grid box was used for  $\beta$ -galactosidase (bovine liver). Docking calculations were performed in the presence of the selected inhibitors using AutoDock Vina at default parameters.[49] Nine conformations were visualized for each of the docked amidines with PYMOL.[46] The conformation with the lowest free energy estimate for each of the inhibitor-enzyme assemblies was chosen for subsequent molecular dynamic studies and exported as pdb file;  $\beta$ -galactosidase (bovine liver) with **1a** (−6.7 kcal/mol), **1v** (−5.9 kcal/mol), and **1x** (−5.3 kcal/mol);  $\beta$ -galactosidase (*A. oryzae*) with **1a** (−7.1 kcal/mol), **1v** (−6.9 kcal/mol), and **1x** (−5.8 kcal/mol).

#### **4.2.4.2. Molecular dynamic studies of glycosidases with coordinated galactonoamidine**

**inhibitors:** All molecular dynamic simulations were performed with GROMACS 4.6.7.[50] The GROMACS coordinate (“gro”) and topology (“top”) files of the enzymes were produced with pdb2gmx and the GROMOS96 43A1 force field.[33] The inhibitor conformation with the lowest free energy, as predicted by AutoDock Vina, was exported as a pdb file and submitted to the PRODRG server to obtain the coordinate (“gro”) and topology (“itp”) files.[51] It has been recognized that the partial charges produced by PRODRG lead to artifacts when used with the GROMOS force field.[52] The partial charges of the inhibitors were thus edited based on a best practice approach suggested by Lemkul.[52] The enzyme-inhibitor assembly was simulated using the combined gro and topology files based on the configuration predicted by Autodock Vina.[53]

The complex derived from  $\beta$ -galactosidase (bovine liver) and the selected inhibitors were solvated with 41945–41956 water molecules in a  $1367 \text{ nm}^3$  cubic box using the single point charge (SPC) model.[54] Likewise, the corresponding complexes from the inhibitors and  $\beta$ -galactosidase (*A. oryzae*) were solvated with 75208–75214 SPC water molecules in a slightly larger  $2389 \text{ nm}^3$  cubic box. Subsequently, random water molecules were replaced by sodium ions to neutralize the system, i.e. for  $\beta$ -galactosidase (bovine liver): 1  $\text{Na}^+$  and for  $\beta$ -galactosidase (*A. oryzae*): 28  $\text{Na}^+$ . The solvated enzyme-inhibitor complexes were then minimized using the steepest-descent method to remove possible steric clashes.[33] Afterward, a NVT simulation at 303K over 100 ps and a NPT simulation at 1 bar over 500 ps were performed using the stochastic rescaling thermostat.[55] Last, a 31 ns NPT simulation was performed using the Nosé-Hoover thermostat [56] with a relaxation time of 2.0 ps and the Parrinello-Rahman barostat [57] with a relaxation time of 5.0 ps. The final 30 ns of the NPT simulation were treated as production trajectories for data analyses.

All molecular dynamic studies were carried out using a 2 fs time step size. The Coulomb interactions were treated with the particle-mesh Ewald method with a real space cutoff of 12 Å and a fourth-order spline with a Fourier grid spacing of 1.3 Å.[58, 59] Lennard-Jones interactions were also cut off at 12 Å.[60] All bond lengths were constraint using a fourth order LINCS algorithm.[61] The number of H-bonds was determined using the H-bond plugin implemented in the Visual Molecular Dynamics (VMD) program with a cut-off distance for donor-acceptor interactions of ~ 3.0 Å and a cut-off angle for donor-H atom-acceptor assemblies of 20°.[62]

## Supplementary Material

Refer to Web version on PubMed Central for supplementary material.

## Acknowledgments

Support of this research to F. W. by the National Institutes of Health (1R01GM120578) and to S. S. by the National Science Foundation (CHE-1305543) and the Arkansas Biosciences Institute is gratefully acknowledged. The facilities used in this study were supported by Grant Number P30 GM103450 from the National Institute of General Medical Sciences (NIGMS) of the National Institutes of Health (NIH). The molecular dynamics simulations were performed in the Arkansas High-Performance Computing Center, which is supported by the National Science Foundation (ACI0722625, ACI0959124, ACI0963249, and ACI0918970) and the Division of Science and Technology at the Arkansas Economic Development Commission.

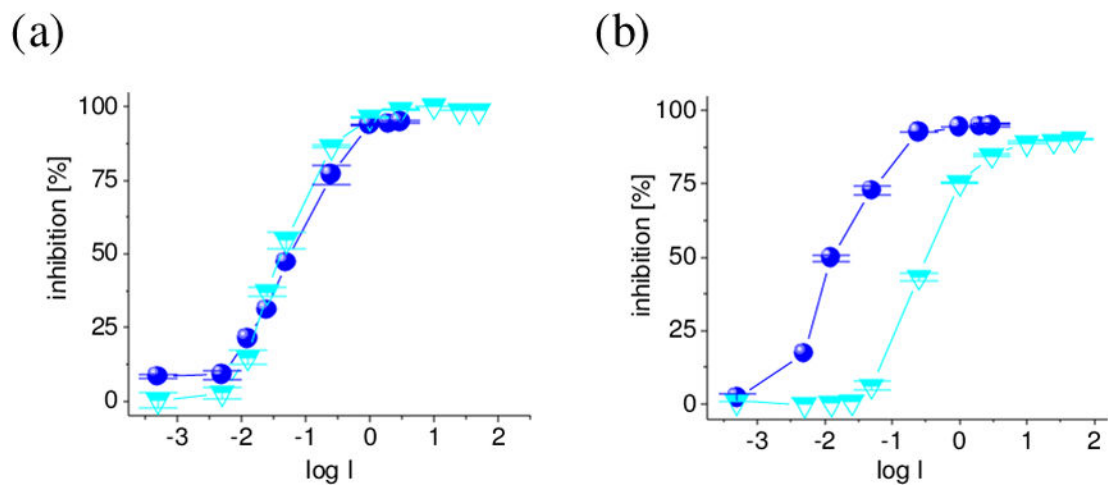
## References

1. Cantarel BL, Coutinho PM, Rancurel C, Bernard T, Lombard V, Henrissat B. The Carbohydrate-Active EnZymes database (CAZy): an expert resource for Glycogenomics. *Nucleic Acids Res.* 2009; 37:D233–D238. [PubMed: 18838391]
2. Lombard V, Golaconda Ramulu H, Drula E, Coutinho PM, Henrissat B. The carbohydrate-active enzymes database (CAZy) in 2013. *Nucleic Acids Res.* 2014; 42:D490–495. [PubMed: 24270786]
3. Juers DH, Huber RE, Matthews BW. Structural comparisons of TIM barrel proteins suggest functional and evolutionary relationships between b-galactosidase and other glycohydrolases. *Protein Sci.* 1999; 8:122–136. [PubMed: 10210191]
4. Konno H, Katoh K. An extracellular  $\beta$ -galactosidase secreted from cell suspension cultures of carrot. Its purification and involvement in cell wall-polysaccharide hydrolysis. *Physiol Plant.* 1992; 85:507–514.
5. Maksimainen MM, Lampio A, Mertanen M, Turunen O, Rouvinen J. The Crystal structure of acidic  $\beta$ -galactosidase from *Aspergillus oryzae*. *Int J Biol Macromolec.* 2013; 60:109–115.
6. Juers DH, Heightman TD, Vasella A, McCarter JD, Mackenzie L, Withers SG, Matthews BW. A structural view of the action of *Escherichia coli* (lac Z)  $\beta$ -galactosidase. *Biochemistry.* 2001; 40:14781–14794. [PubMed: 11732897]
7. DiCioccio RA, Barlow J, Maria JK. Purification of a b-D-galactosidase from Bovine Liver by affinity chromatography. *Carbohydr Res.* 1984; 127:109–120. [PubMed: 6424938]
8. Gloster TM, Davies GJ. Glycosidase inhibition: assessing mimicry of the transition state. *Org Biomol Chem.* 2010; 8:305–320. [PubMed: 20066263]
9. Henrissat B, Davies G. Structural and sequence-based classification of glycoside hydrolases. *Curr Opin Struct Biol.* 1997; 7:637–644. [PubMed: 9345621]
10. Berman HM, Westbrook J, Feng Z, Gilliland G, Bhat TN, Weissig H, Shindyalov IN, Bourne PE. The Protein Data Bank. *Nucleic Acids Res.* 2000; 28:235–242. [PubMed: 10592235]
11. Greenfield NJ. Using circular dichroism spectra to estimate protein secondary structure. *Nat Protoc.* 2006; 1:2876–2890. [PubMed: 17406547]
12. Froehlich RFG, Furneaux RH, Mahuran DJ, Saf R, Stuetz AE, Tropak MB, Wicki J, Withers SG, Wrodnigg TM. 1-Deoxy-D-galactonojirimycins with dansyl capped N-substituents as  $\beta$ -

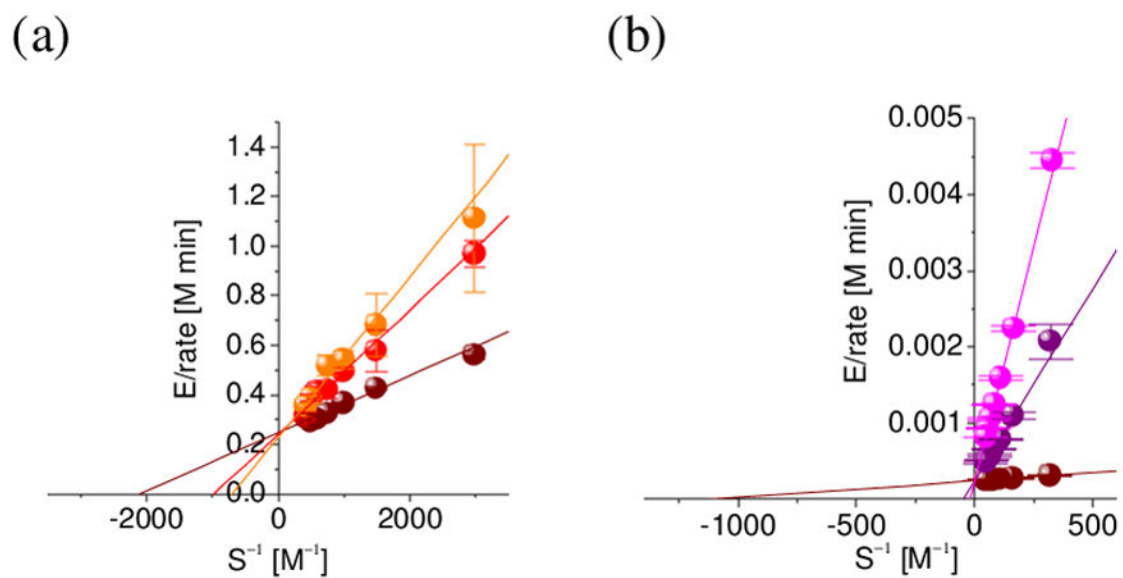
- galactosidase inhibitors and potential probes for GM1 gangliosidosis affected cell lines. *Carbohydr Res.* 2011; 346:1592–1598. [PubMed: 21645885]
13. Hollander P, Pi-Sunyer X, Coniff RF. Acarbose in the treatment of type I diabetes. *Diabetes Care.* 1997; 20:248–253. [PubMed: 9051366]
  14. Magini A, Polchi A, Tozzi A, Tancini B, Tantucci M, Urbanelli L, Borsello T, Calabresi P, Emiliani C. Abnormal cortical lysosomal b-hexosaminidase and b-galactosidase activity at post synaptic sites during Alzheimer's disease progression. *Int J Biochem Cell Biol.* 2015; 58:62–70. [PubMed: 25462158]
  15. Jenkins J, Leggio LL, Harris G, Pickersgill R.  $\beta$ -glucosidase,  $\beta$ -galactosidase, family A cellulases, Family F xylanases and two barley glycanases form a superfamily of enzymes with 8-fold b/a architecture and with two conserved glutamates near the carboxy-terminal ends of  $\beta$ -strands four and seven. *FEBS Lett.* 1995; 362:281–285. [PubMed: 7729513]
  16. Fan QH, Claunch KA, Striegler S. Structure-activity relationship of highly potent galactonoamidine inhibitors toward  $\beta$ -galactosidase (*Aspergillus oryzae*). *J Med Chem.* 2014; 57:8999–9009. [PubMed: 25295392]
  17. Kanso R, Yancey EA, Striegler S. N-Benzylgalactonoamidines as potent b-galactosidase inhibitors. *Tetrahedron.* 2012; 68
  18. Fan QH, Striegler S, Langston RG, Barnett JD. Evaluating N-benzylgalactonoamidines as putative transition state analogs for  $\beta$ -galactoside hydrolysis. *Org Biomol Chem.* 2014; 12:2792–2800. [PubMed: 24668069]
  19. Ganem B. Inhibitors of carbohydrate-processing enzymes: Design and synthesis of sugar-shaped heterocycles. *Acc Chem Res.* 1996; 29:340–347.
  20. Leatherbarrow RJ. Using linear and non-linear regression to fit biochemical data. *Trends Biochem Sci.* 1990; 15:455–458. [PubMed: 2077683]
  21. Huang HL, Krieger IV, Parai MK, Gawandi VB, Sacchettini JC. Mycobacterium tuberculosis Malate Synthase Structures with Fragments Reveal a Portal for Substrate/Product Exchange. *J Biol Chem.* 2016; 291:27421–27432. [PubMed: 27738104]
  22. Pala D, Rivara S, Mor M, Milazzo FM, Roscilli G, Pavoni E, Giannini G. Kinetic analysis and molecular modelling of the inhibition mechanism of roneparstat (SST0001) on human heparanase. *Glycobiology.* 2016:cww003.
  23. O'Rourke KF, Jelowicki AM, Boehr DD. Controlling Active Site Loop Dynamics in the ( $\beta/\alpha$ ) 8 Barrel Enzyme Indole-3-Glycerol Phosphate Synthase. *Catalysts.* 2016; 6:129.
  24. Kohen A. Dihydrofolate reductase as a model for studies of enzyme dynamics and catalysis. *F1000Res.* 2015; 4
  25. Wang LH, Wang MS, Zeng XA, Gong DM, Huang YB. An in vitro investigation of the inhibitory mechanism of  $\beta$ -galactosidase by cinnamaldehyde alone and in combination with carvacrol and thymol. *Biochim Biophys Acta.* 2017; 1861:3189–3198. [PubMed: 27531708]
  26. Soto D, Escobar S, Guzmán F, Cárdenas C, Bernal C, Mesa M. Structure-activity relationships on the study of  $\beta$ -galactosidase folding/unfolding due to interactions with immobilization additives: Triton X-100 and ethanol. *Int J Biol Macromolec.* 2017; 96:87–92.
  27. Louis-Jeune C, Andrade-Navarro MA, Perez-Iratxeta C. Prediction of protein secondary structure from circular dichroism using theoretically derived spectra. *Proteins: Struct, Funct, Bioinf.* 2012; 80:374–381.
  28. Micsonai A, Wien F, Kernya L, Lee YH, Goto Y, Réfrégiers M, Kardos J. Accurate secondary structure prediction and fold recognition for circular dichroism spectroscopy. *P Natl Acad Sci USA.* 2015; 112:E3095–E3103.
  29. Kim DE, Chivian D, Baker D. Protein structure prediction and analysis using the Robetta server. *Nucleic Acids Research.* 2004; 32:W526–W531. [PubMed: 15215442]
  30. Kaufmann KW, Lemmon GH, DeLuca SL, Sheehan JH, Meiler J. Practically useful: what the Rosetta protein modeling suite can do for you. *Biochemistry.* 2010; 49:2987–2998. [PubMed: 20235548]
  31. Benkert P, Biasini M, Schwede T. Toward the estimation of the absolute quality of individual protein structure models. *Bioinformatics.* 2010; 27:343–350. [PubMed: 21134891]

32. Benkert P, Tosatto SC, Schomburg D. QMEAN: A comprehensive scoring function for model quality assessment. *Proteins: Structure, Function, and Bioinformatics*. 2008; 71:261–277.
33. Scott WR, Hünenberger PH, Tironi IG, Mark AE, Billeter SR, Fennen J, Torda AE, Huber T, Krüger P, van Gunsteren WF. The GROMOS biomolecular simulation program package. *J Phys Chem A*. 1999; 103:3596–3607.
34. Cagir A, Tao ZF, Sucheck SJ, Hecht SM. Solid-phase synthesis and biochemical evaluation of conformationally constrained analogues of deglycobleomycin A 5. *Bioorganic & medicinal chemistry*. 2003; 11:5179–5187. [PubMed: 14604681]
35. Ibrahim DA, Boucau J, Lajiness DH, Veleti SK, Trabbic KR, Adams SS, Ronning DR, Sucheck SJ. Design, synthesis, and X-ray analysis of a glycoconjugate bound to Mycobacterium tuberculosis antigen 85C. *Bioconjug Chem*. 2012; 23:2403–2416. [PubMed: 23190459]
36. Papandreou G, Tong M, Ganem B. Amidine, Amidrazone, and Amidoxime Derivatives of Monosaccharide Aldonolactams: Synthesis and Evaluation as Glycosidase Inhibitors. *Journal of American Chemical Society*. 1993; 115:11682–11690.
37. Dugdale ML, Dymianiw DL, Minhas BK, D'Angelo I, Huber RE. Role of Met-542 as a guide for the conformational changes of Phe-601 that occur during the reaction of  $\beta$ -galactosidase (*Escherichia coli*). *Biochem Cell Biol*. 2010; 88:861–869. [PubMed: 20921997]
38. Juers DH, Jacobson RH, Wigley D, Zhang XJ, Huber RE, Tronrud DE, Matthews BW. High-resolution refinement of  $\beta$ -galactosidase in a new crystal form reveals multiple metal binding sites and provides a structural basis for a-complementation. *Protein Sci*. 2000; 9:1695–1699.
39. Fan QH, Pickens JB, Striegler S, Gervaise CD. Illuminating the binding interactions of galactonoamidines during the inhibition of  $\beta$ -galactosidase (*E. coli*). *Bioorg Med Chem*. 2016; 24:661–671. [PubMed: 26740154]
40. Notenboom V, Birsan C, Warren RAJ, Withers SG, Rose DR. Exploring the Cellulose/Xylan Specificity of the  $\beta$ -1,4-Glycanase Cex from *Cellulomonas fimi* through Crystallography and Mutation. *Biochemistry*. 1998; 37:4751–4758. [PubMed: 9537990]
41. Wacker M, Feldman MF, Callewaert N, Kowarik M, Clarke BR, Pohl NL, Hernandez M, Vines ED, Valvano MA, Whitfield C. Substrate specificity of bacterial oligosaccharyltransferase suggests a common transfer mechanism for the bacterial and eukaryotic systems. *Proceedings of the National Academy of Sciences*. 2006; 103:7088–7093.
42. Walker, JM. The Bicinchoninic Acid (BCA) Assay for Protein Quantitation. In: Walker, JM., editor. *Basic Protein and Peptide Protocols*. Humana Press; Totowa, NJ: 1994. p. 5-8.
43. Kanso R, Striegler S. Multi gram-scale synthesis of galactothionolactam and its transformation into a galactonoamidine. *Carbohydr Res*. 2011; 346:897–904. [PubMed: 21470597]
44. Harhay GP, Sonstegard TS, Keele JW, Heaton MP, Clawson ML, Snelling WM, Wiedmann RT, Van Tassell CP, Smith TP. Characterization of 954 bovine full-CDS cDNA sequences. *BMC Genomics*. 2005; 6:166. [PubMed: 16305752]
45. Machida M, Asai K, Sano M, Tanaka T, Kumagai T, Terai G, Kusumoto KI, Arima T, Akita O, Kashiwagi Y. Genome sequencing and analysis of *Aspergillus oryzae*. *Nature*. 2005; 438:1157–1161. [PubMed: 16372010]
46. DeLano, W. The PyMOL molecular graphics system on the World Wide Web. 2002. Available at: <http://www.pymol.org>
47. Sanner MF. Python: A programming language for software integration and development. *J Mol Graphics Mod*. 1999; 17:305–320.
48. Morris GM, Huey R, Lindstrom W, Sanner MF, Belew RK, Goodwill DS, Olson AJ. AutoDock4 and AutoDockTools4: Automated docking with selective receptor flexibility. *J Comput Chem*. 2009; 30:2785–2791. [PubMed: 19399780]
49. Trott O, Olson AJ. Software news and update AutoDock Vina: Improving the speed and accuracy of docking with a new scoring function, efficient optimization, and multithreading. 2009:455–461.
50. Hess B, Kutzner C, Van Der Spoel D, Lindahl E. GROMACS 4: algorithms for highly efficient, load-balanced, and scalable molecular simulation. *J Chem Theory Comput*. 2008; 4:435–447. [PubMed: 26620784]
51. Schuttelkopf AW, van Aalten DMF. PRODRG: a tool for high-throughput crystallography of protein-ligand complexes. *Acta Crystallogr D*. 2004; 60:1355–1363. [PubMed: 15272157]

52. Lemkul JA, Allen WJ, Bevan DR. Practical considerations for building GROMOS-compatible small-molecule topologies. *J Chem Inf Model.* 2010; 50:2221–2235. [PubMed: 21117688]
53. Pol-Fachin L, Fernandes CL, Verli H. GROMOS96 43a1 performance on the characterization of glycoprotein conformational ensembles through molecular dynamics simulations. *Carbohydr Res.* 2009; 344:491–500. [PubMed: 19185293]
54. Berendsen H, Grigera J, Straatsma T. The missing term in effective pair potentials. *J Phys Chem.* 1987; 91:6269–6271.
55. Bussi G, Donadio D, Parrinello M. Canonical sampling through velocity rescaling. *J Chem Phys.* 2007; 126:014101. [PubMed: 17212484]
56. Nose S. Constant-temperature molecular dynamics. *J Phys Condens Matter.* 1990; 2:SA115.
57. Ray JR, Rahman A. Statistical ensembles and molecular dynamics studies of anisotropic solids. *J Chem Phys.* 1984; 80:4423–4428.
58. Darden T, York D, Pedersen L. Particle mesh Ewald: An  $N \log(N)$  method for Ewald sums in large systems. *J Chem Phys.* 1993; 98:10089–10092.
59. Essmann U, Perera L, Berkowitz ML, Darden T, Lee H, Pedersen LG. A smooth particle mesh Ewald method. *J Chem Phys.* 1995; 103:8577–8593.
60. Verlet L. Computer "experiments" on classical fluids. I. Thermodynamical properties of Lennard-Jones molecules. *Phys Rev.* 1967; 159:98.
61. Hess B, Bekker H, Berendsen HJ, Fraaije JG. LINCS: a linear constraint solver for molecular simulations. *J Comput Chem.* 1997; 18:1463–1472.
62. Humphrey W, Dalke A, Schulten K. VMD-Visual Molecular Dynamics. *J Molec Graphics.* 1996; 14:33–38.

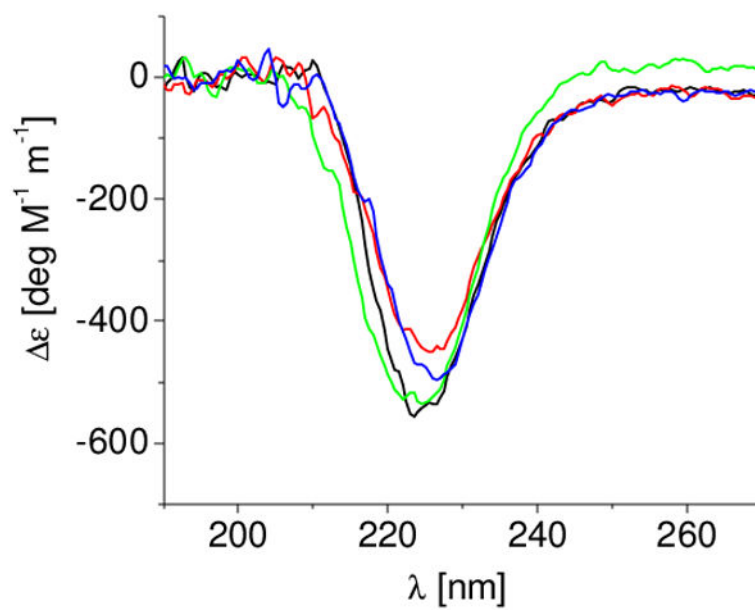


**Figure 1.** Efficacy of the inhibition of  $\beta$ -galactosidases from bovine liver (solid blue circle) and *A. oryzae* (open cyan triangle) during substrate hydrolysis in presence of galactonoamidines (a) **1d**; and (b) **1h**; I in nM.

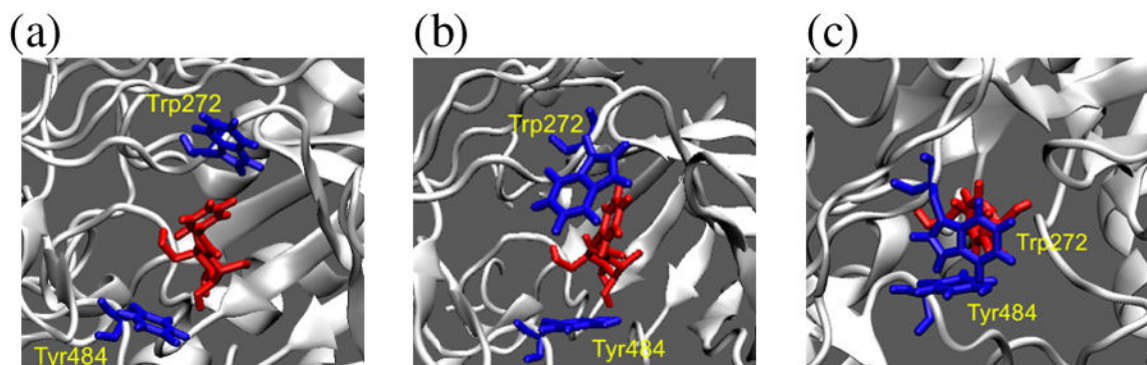


**Figure 2.** Lineweaver-Burk plots depicting competitive inhibition of the hydrolysis of model substrates by **1a** for (a)  $\beta$ -galactosidase (bovine liver) in presence of 0 nM (wine), 0.05nM (red) and 0.075 nM (orange) inhibitor concentrations; and (b)  $\beta$ -galactosidase (*A. oryzae*) at 0 nM (wine), 0.05nM (purple) and 0.075 nM (magenta) inhibitor concentrations.

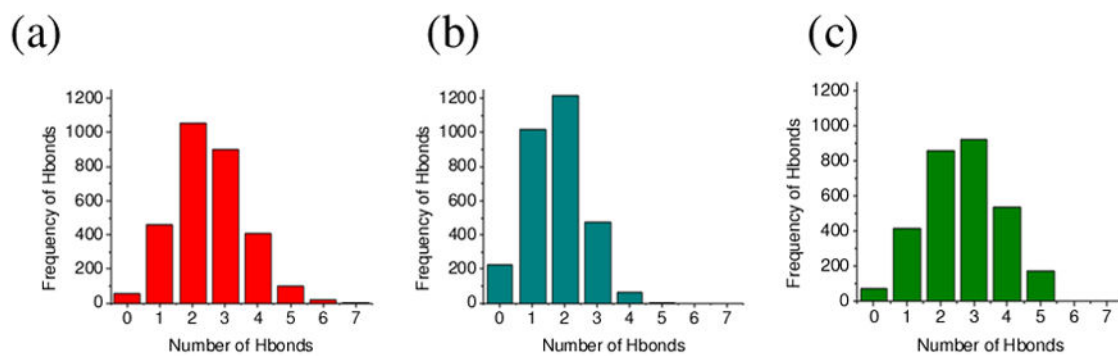




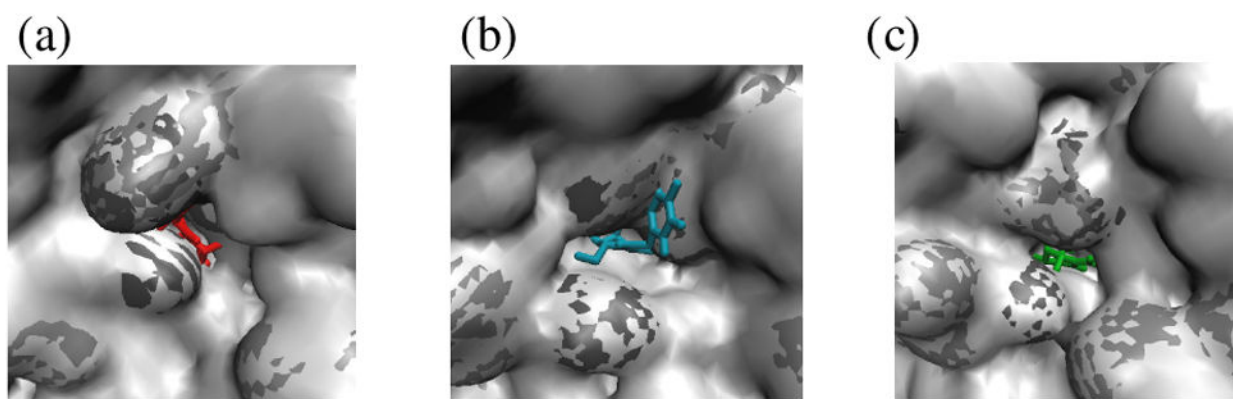
**Figure 3.** CD spectra of  $\beta$ -galactosidase (bovine liver) (a) without inhibitor (black,  $\lambda_{\max} = 224$  nm); in presence of (b) **1a** (red,  $\lambda_{\max} = 225$  nm), (c) **1v** (blue,  $\lambda_{\max} = 225$  nm); and (d) **1x** (green,  $\lambda_{\max} = 227$  nm).



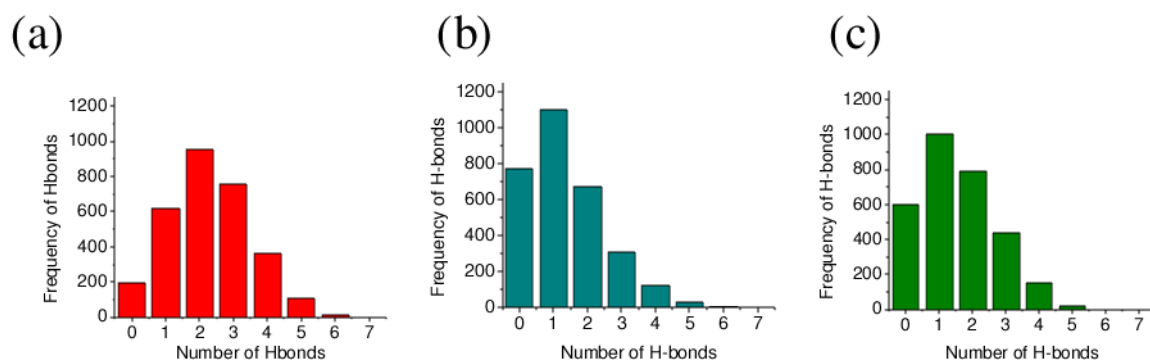
**Figure 4.** Snapshots of the induced fit of **1a** in the active site of  $\beta$ -galactosidase (bovine liver) (a) before, (b) during and (c) after loop closure.



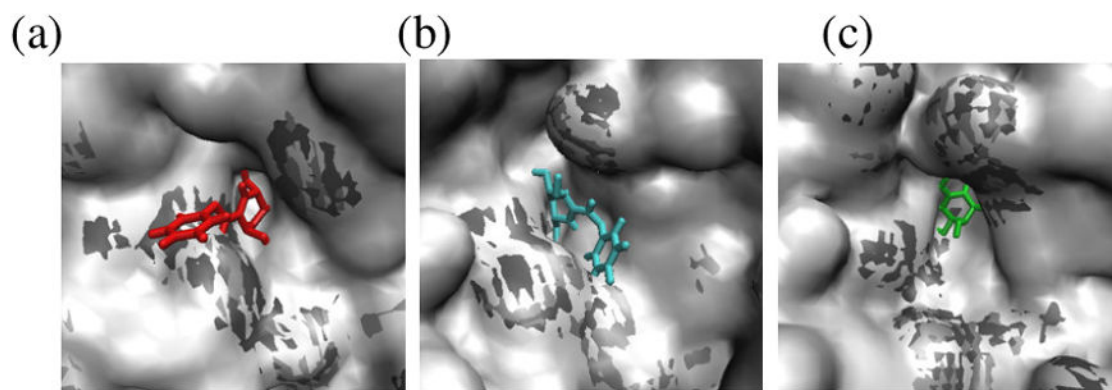
**Figure 5.** Number of H-bonds in correlation to their occurrence for  $\beta$ -galactosidase (bovine liver) in presence of (a) **1a**, (b) **1v**, and (c) **1x** as observed by molecular dynamics simulations over 30ns



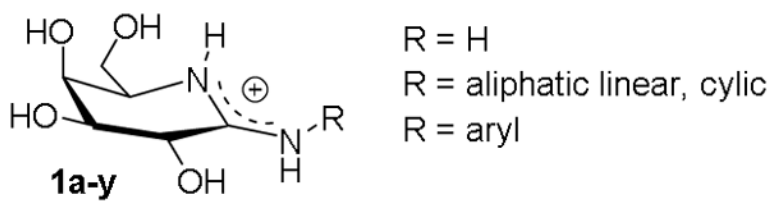
**Figure 6.** Active site of  $\beta$ -galactosidase (bovine liver) with coordinated galactonoamidines (a) **1a**, (b) **1v**, and (c) **1x** extracted from the molecular dynamic studies.



**Figure 7.** Number of H-bonds in correlation to their occurrence for  $\beta$ -galactosidase (*A. oryzae*) in presence of (a) **1a**, (b) **1v**, and (c) **1x** as observed by molecular dynamics simulations over 30ns



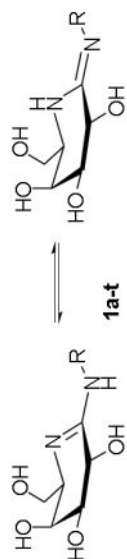
**Figure 8.** Active site of  $\beta$ -galactosidase (*A. oryzae*) with coordinated galactonoamidines (a) **1a**, (b) **1v**, and (c) **1x** extracted from the molecular dynamic studies.



**Chart 1.**  
Galactonoamidines **1a-y** at assay conditions

Inhibition of the hydrolysis of model substrates by  $\beta$ -galactosidases from bovine liver (5 mM HEPES buffer, pH 7.50;  $k_{\text{cat}} = 4.24 \pm 0.26$  [ $\text{min}^{-1}$ ];  $K_M = 0.51 \pm 0.01$  mM) and *A. oryzae* (50 mM acetate buffer, pH 5.00;  $k_{\text{cat}} = 2400 \pm 140$  [ $\text{min}^{-1}$ ];  $K_M = 0.70 \pm 0.01$  mM) in the presence of galactonoamidines **1a-t**.

Table 1

Chart 1, Structures of galactonoamidines **1a-t**

Compound	Aglycon R	$\beta$ -galactosidase (Bovine Liver)		$\beta$ -galactosidase ( <i>A. oryzae</i> ) [16]	
		$K_i \pm K_i$ [nM]	IC <sub>50</sub> [nM]	$K_i \pm K_i$ [nM]	IC <sub>50</sub> [nM]
<i>Aromatic aglycon, parent structure</i>					
<b>1a</b>		$0.05 \pm 0.01$	18.9	$21.1 \pm 1.2$	49
<i>Aromatic aglycon with electron-donating substituents</i>					
<b>1b</b>		$0.20 \pm 0.02$	118	$23.6 \pm 2.4$	623
<b>1c</b>		$0.11 \pm 0.01$	16.2	$29.4 \pm 5.2$	131
<b>1d</b>		$0.07 \pm 0.01$	57.6	$8.0 \pm 0.5$	36



Author Manuscript

Author Manuscript

Author Manuscript

Author Manuscript



Chart 1. Structures of galactonoamidines **1a-t**

Compound	Aglycon R	$\beta$ -galactosidase (Bovine Liver)			IC <sub>50</sub> [nM]	K <sub>i</sub> ± K <sub>i</sub> [nM]	K <sub>i</sub> ± K <sub>i</sub> [nM]	IC <sub>50</sub> [nM]
		K <sub>i</sub> ± K <sub>i</sub> [nM]	IC <sub>50</sub> [nM]	K <sub>i</sub> ± K <sub>i</sub> [nM]				
<b>1e</b>		0.11 ± 0.01	412	20.6 ± 2.5	122			
<i>Aromatic aglycon with electron-withdrawing substituents</i>								
<b>1f</b>		0.23 ± 0.01	43.1	16.1 ± 0.3	117			
<b>1g</b>		0.13 ± 0.02	9.4	20.3 ± 2.3	115			
<b>1h</b>		0.19 ± 0.02	9.1	10.1 ± 2.5	331			
<b>1i</b>		0.16 ± 0.01	15.2	15.7 ± 0.1	122			
<b>1j</b>		0.12 ± 0.01	26.2	17.1 ± 3.4	150			

*Cyclic aliphatic aglycon with methylene spacer*



Chart 1. Structures of galactonoamimidines 1a-t

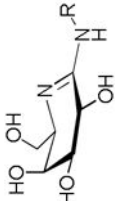
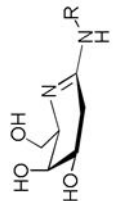
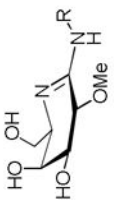
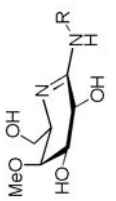
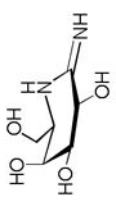
Compound	Aglycon R	$\beta$ -galactosidase (Bovine Liver)			IC <sub>50</sub> [nM]	K <sub>i</sub> ± K <sub>i</sub> [nM]	K <sub>i</sub> ± K <sub>i</sub> [nM]	IC <sub>50</sub> [nM]
		K <sub>i</sub> ± K <sub>i</sub> [nM]	IC <sub>50</sub> [nM]	K <sub>i</sub> ± K <sub>i</sub> [nM]				
1k		0.39 ± 0.07	> 1400	9.5 ± 1.1	36			
1l		0.08 ± 0.01	11.6	11.3 ± 0.9	22			
1m		0.16 ± 0.03	45.4	6.3 ± 0.6	36			
<i>Linear aliphatic aglycon with aromatic end group or branching</i>								
1n		0.32 ± 0.02	1030	149 ± 2	226			
1o		0.11 ± 0.01	24.1	10.8 ± 0.7	107			
1p		0.24 ± 0.03	42.7	48.4 ± 3.3	33.5			
1q		0.18 ± 0.02	21.6	7.8 ± 1.4	36			

Chart 1. Structures of galactonoamidines **1a-t**

Compound	Aglycon R	$\beta$ -galactosidase (Bovine Liver)			IC <sub>50</sub> [nM]	IC <sub>50</sub> [nM]
		K <sub>i</sub> ± K <sub>i</sub> [nM]	K <sub>i</sub> ± K <sub>i</sub> [nM]	K <sub>i</sub> ± K <sub>i</sub> [nM]		
<b>1r</b>		0.06 ± 0.01	41.3	8.6 ± 1.2		36
<i>Cyclic aliphatic without spacer</i>						
<b>1s</b>		0.32 ± 0.02	> 1000	31.9 ± 1.8		369
<b>1t</b>		2.34 ± 0.30	> 1000	602 ± 52		4870

Table 2

Inhibition of the hydrolysis of model substrates by  $\beta$ -galactosidases from bovine liver (5 mM HEPES buffer, pH 7.50) and *A. oryzae* (50 mM acetate buffer, pH 5.00) in the presence of galactonoamidines **1d**, **1u–y**; R =  $-\text{CH}_2-\text{C}_6\text{H}_4-\text{CH}_3$

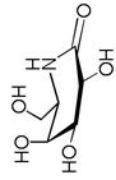
Compound	Glycon structure	$\beta$ -galactosidase (Bovine Liver)		$\beta$ -galactosidase ( <i>A. oryzae</i> )	
		$K_i \pm K_i$ [nM]	IC <sub>50</sub> [nM]	$K_i \pm K_i$ [nM]	IC <sub>50</sub> [nM]
<i>Galactonoamidines with modifications in the glycon</i>					
<b>1d</b>		0.07 ± 0.01	57.6	8.0 ± 0.5	36
<b>1u</b>		0.60 ± 0.07	850	2,400 ± 300	33,300
<b>1v</b>		1,500 ± 220	10,800	3,400 ± 300	41,400
<b>1w</b>		840 ± 60	9,200	1,400 ± 200	40,700
<i>Control compounds</i>					
<b>1x</b>		2,000 ± 200	> 50,000	150 ± 20	830

Author Manuscript

Author Manuscript

Author Manuscript

Author Manuscript

Compound	Glycon structure	$\beta$ -galactosidase (Bovine Liver)		$\beta$ -galactosidase ( <i>A. oryzae</i> )			
		$K_i \pm$	$K_i$ [nM]	$K_i \pm$	$K_i$ [nM]	$IC_{50}$ [nM]	$IC_{50}$ [nM]
<b>1y</b>		$2,700 \pm 260$	8,700	$615 \pm 30$	$615 \pm 30$	$> 50,000$	$> 50,000$